Physica E 159 (2024) 115909

Contents lists available at ScienceDirect

Physica E: Low-dimensional Systems and Nanostructures

journal homepage: www.elsevier.com/locate/physe

Evidence of ferromagnetic behaviour in carbon nanospheres synthesised by the chemical vapour deposition technique

Othmane Mouane [a,*], Elias Sideras-Haddad [a,b], Daniel Wamwangi [a,b], Victor Mashindi [c], Gerrard Peters [a,b], Rudolph M. Erasmus [a,b], Deena Naidoo [a,b], Theodoros Gkanetsos [d], Neil J. Coville [b,c]

[a] School of Physics, University of the Witwatersrand, Wits 2050, Johannesburg, South Africa
[b] DSI-NRF Centre of Excellence in Strong Materials, University of the Witwatersrand, Wits 2050, Johannesburg, South Africa
[c] Molecular Sciences Institute, School of Chemistry, University of the Witwatersrand, Wits 2050, Johannesburg, South Africa
[d] Department of Industrial Design and Production Engineering, School of Engineering - University of West Attica, Greece

ARTICLE INFO

Keywords:
Carbon nanospheres
Ferromagnetism
Super-paramagnetism
Variable range hoping

ABSTRACT

The magnetic and electrical properties of two different sets of carbon nanospheres synthesised by chemical vapour deposition were investigated, using a state-of-the-art Physical Property Measurement System (PPMS). Scanning electron microscopy imaging of the carbon nanospheres revealed a difference in size with a diameters distribution of approximately 200–400 nm and 400–500 nm. PPMS magnetic measurements of the 400–500 nm diameter carbon nanospheres exhibited diamagnetism at high temperatures and clear superparamagnetic behaviour at very low temperatures (<10 K). However, ferromagnetism was observed in carbon nanospheres of diameter < 400 nm. The results obtained from both inductively Coupled Plasma Mass Spectrometry and Mössbauer spectroscopy, and as well as the calculated saturation magnetisation indicate that the observed ferromagnetism in the carbon nanospheres of diameter < 400 nm is intrinsic and could not be accounted for by the magnetic impurities such as Fe and Ni introduced during the synthesis process. The electrical properties of a network of carbon nanospheres were investigated and showed a variable range hopping class of conductivity.

1. Introduction

Magnetism in carbon nanomaterials is an interesting and exciting research domain. In general, carbon allotropes exhibit a diamagnetic behaviour with a susceptibility in the range of $-(10^{-4}–10^{-6})$ emu g^{-1} per magnetic field unit [1]. However, several research groups have reported exceptional magnetic behaviour in a variety of carbon materials. Unexpected ferromagnetic characteristics were first observed in pure and polymerised C_{60} at high temperatures around 800 K [2,3]. Another astonishing and unforeseen discovery was the observation of induced ferromagnetic behaviour in Highly Oriented Pyrolytic Graphite (HOPG) following low MeV proton irradiation over a wide range of temperatures [4–9]. The work showed that the magnetisation was not related to ferromagnetic impurities. Furthermore, ferromagnetic-like hysteresis magnetisation loops were observed in additional carbon-based nanomaterials, such as nano-graphite [10], graphene [11,12], carbon encapsulating silver nanoparticles [13], composites of HOPG nanospheres [1], carbon nanofoams [14,15], and microporous carbon [16]. The origin of this anomalous magnetic behaviour observed in carbon-based materials is still unclear and different explanations have been proposed. Numerous research groups have speculated that the manifestation of these unusual magnetic properties are due to vacancies, topographic defects or magnetic frustration [11], positive or negative surface curvatures (such as in graphene), and the chemical nature of the edges such as the mixture of sp^2 and sp^3 hybridised states [13]. The role of hydrogen and oxygen has also been investigated with respect to catalysing the process and inducing the observed magnetic behaviour in the carbon systems [12,13]. Li et al. [1] also reported that morphological characteristics such as crystallinity and size affect the magnetic properties in pyrolytic carbon. Moreover, there was evidence that the magnetism originated from s-p symmetry unpaired electrons at structural defects rather than of d or f electrons of the impurities. Such ferromagnetic properties in carbon nanomaterials can lead to technological breakthroughs in spintronic, telecommunications, and biomedical applications [7,17].

In this research paper, intrinsic ferromagnetic behaviour in carbon nanospheres is reported. The carbon nanospheres synthesised by

* Corresponding author.
E-mail addresses: othmane.mouane@wits.ac.za (O. Mouane), elias.sideras-haddad@wits.ac.za (E. Sideras-Haddad), Daniel.Wamwangi@wits.ac.za (D. Wamwangi).

https://doi.org/10.1016/j.physe.2024.115909
Received 1 March 2023; Received in revised form 6 November 2023; Accepted 29 January 2024
Available online 1 February 2024

Chemical Vapour Deposition were characterised by Scanning Electron Microscopy and Inductively Coupled Plasma Mass Spectrometry. The study included Mössbauer spectroscopy to determine the hyperfine parameters of the carbon nanospheres.

2. Experimental

A non-catalytic horizontal chemical vapour deposition system in the School of Chemistry, University of the Witwatersrand, was used for the synthesis of the carbon nanospheres [18,19]. The setup in use comprised a quartz tube placed in a furnace and was connected to argon and acetylene cylinders separately. The procedure followed in the synthesis of the carbon nanospheres commenced by heating up the furnace to a temperature of 800–900 °C, then argon and acetylene were allowed to flow in the quartz tube at 100 and 200 ml/min respectively for 20 to 40 min [18,19].

The structural and elemental composition of the synthesised carbon nanosphere powders were characterised by scanning electron microscopy (SEM). In addition, trace element analysis with sensitivity of parts per billion level was performed by means of Inductively Coupled Plasma Mass Spectrometry (Perkin Elmer NexION 300). In addition, the samples were characterised by micro-Raman spectroscopy using a Horiba Jobin-Yvon LabRAM HR Raman spectrometer and 514.5 nm emission line of the argon-ion gas laser. The crystallinity of the samples were investigated by X-ray powder diffraction (XRD). The scans were performed using a Rigaku Smartlab diffractometer using Cu Kα_1 radiation (λ_1 = 1.5406 Å), with a resolution of 10°/min in the 2θ range of 10 to 100°.

The electrical and magnetic properties of the synthesised carbon nanosphere powders were measured by a Quantum Design Physical Property Measurement System ("DynaCool" 12 T). The system offers the possibility to conduct measurements at temperatures in the range between 1.8–400 K using high precision magnetic fields in the range between +/− 12 T.

The magnetic properties were investigated by a DC-Vibrating Sample Magnetometer (VSM). Prior to the measurements, the mass of the carbon powders were carefully measured (12 mg) with an electronic balance thereafter the samples were transferred to a poly-carbonate capsule and fitted in the gold coated brass holder. The sample holder was then connected to the VSM probe and loaded onto the PPMS for calibration measurement and analysis.

The resistance measurement method consisted of a linear four-point probes system. The probes were four spring loaded contacts in a single row plastic body as shown in Fig. 1. Electrical contact with the sample was made by means of rounded tips mounted on springs. The sample used for the measurements was a pressed pellet of carbon nanospheres powder only. The pellet in the form of a disc shape had a diameter and thickness of 10 mm and 1 mm, respectively. The rounded tips and springs prevented damage to the surface of the pellet by applying uniform forces once the spring loaded contacts were in contact with the sample.

The magnetic splitting due to possible Fe impurities in the synthesised carbon nanosphere powders was investigated by means of Mössbauer spectroscopy in transmission mode. The system was equipped with a 10 mCi ^{57}Co (Rh) source, emitting gamma rays periodically toward the carbon nanospheres sample over a succession of velocities. The transmitted radiation from the sample was recorded at room temperature as function of the source velocity for more than five weeks (over 10,000 counts to ensure a small statistical error).

3. Results and discussion

3.1. Structural and elemental composition

High magnification SEM analysis was performed on two sets of carbon nanospheres (A and B) that revealed nanostructures with spherical morphologies with a diameter distribution of approximately 200–400 nm (A) and 400–500 nm (B) as seen in Fig. 2. The SEM imaging of

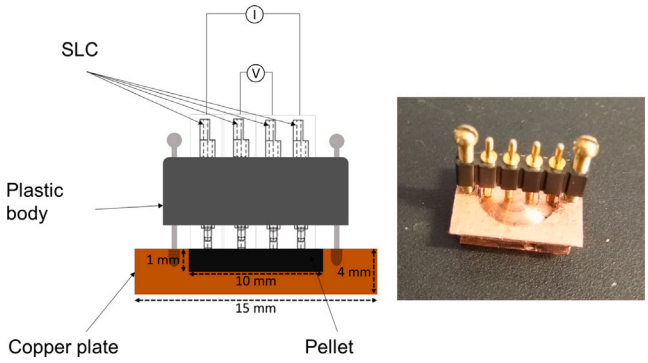

Fig. 1. Sketch (left) and picture (right) of the system used for acquiring the electronic measurements with PPMS. The sketch shows the positioning of the Spring-Loaded Contacts (SLCs) distanced from each other by 2.54 mm and with rounded tips of 1.07 mm diameters. The orientation of the applied voltage and the measured current within the SLCs is shown too.

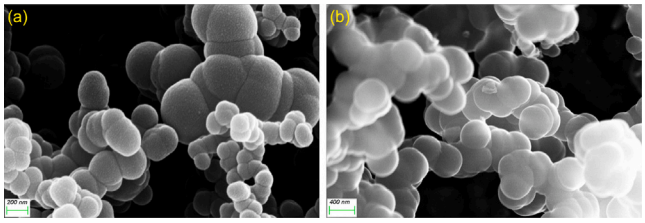

Fig. 2. (a) and (b) are high magnification SEM images of carbon nanospheres powder of samples (A) and (B), respectively. The images show the necklace-like structures of the carbon nanospheres of diameters of 200–400 nm (A) and 400 nm (B).

Table 1
Summary of the inductively coupled plasma mass spectrometry elemental analysis in parts per million (ppm).

Sample	Mg	V	Cr	Mn	Fe	Co	Ni	Cu
"A"	91	9	4	1	126	0	3	1
"B"	16	8	0	0	20	0	0	1

the synthesised carbon nanospheres shows that they are not dispersed but are packed in necklace-like and foam-like structures.

Subsequent energy-dispersive X-ray spectroscopy analysis of these carbon nanospheres revealed the presence of carbon only (not shown here), with no other elemental impurities detected within the sensitivity limits of the measurements (at the few parts per thousand sensitivity level).

In addition, trace element analysis with sensitivity at parts per billion level was performed by means of Inductively Coupled Plasma Mass Spectrometry on both samples "A" and "B". The main concern and focus were on the possible presence of elemental impurities that are magnetic. The Inductively Coupled Plasma Mass Spectrometry scan was tuned to detect the following elements: ^{24}Mg, ^{51}V, ^{52}Cr, ^{55}Mn, ^{56}Fe, ^{59}Co, ^{60}Ni and, ^{63}Cu. The elemental composition is summarised in Table 1.

As can be seen, the metal contaminants detected are less than 10 ppm in both samples except for ^{24}Mg, and ^{56}Fe impurities. These elements were detected in high quantities in sample "A" in comparison to sample "B". For example, in sample "A", the amount of ^{56}Fe detected was 126 ppm, compared to 20 ppm in sample "B".

The recorded Raman spectra for samples "A" and "B" are presented in Fig. 3 which are very similar to Raman spectra of carbon nanospheres reported in the literature [20,21]. At low wavenumbers (500–2000 cm^{-1}), the Raman spectra are fitted using four Voigt curves, which correspond to the D*, D, D″ and G bands. The G band of samples "A" and "B", which are associated with the E_{2g} vibrations of

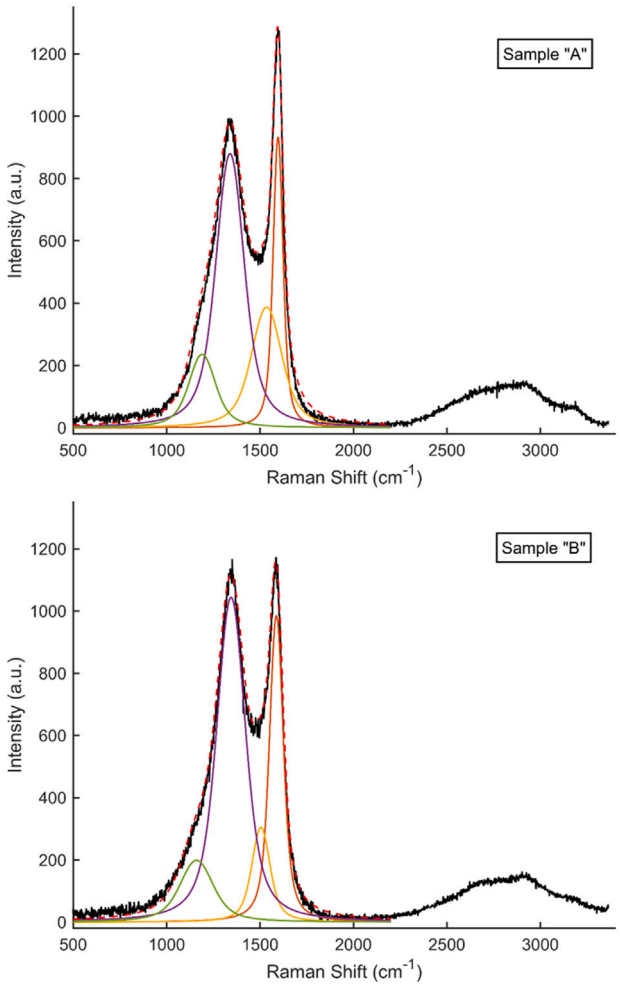

Fig. 3. Full Raman spectra for carbon nanospheres samples "A" and "B" obtained with a 514 nm laser. At the low wavenumbers, the fit shows four Voigt curves which correspond to D*, D, D″ and G bands, respectively (from left to right). The red dashed lines are the convolution of the four curves.

sp^2 sites, are narrow and sited at 1596 and 1587 cm^{-1}, respectively. The observed D band, which represents the double resonant processes near the K point of the Brillouin zone, is associated with the presence of disorder and defects in carbon-based materials. The D band of the two samples is positioned in the range between 1339 and 1345 cm^{-1}. In addition to the G and D bands, the deconvoluted spectra reveal the presence of two more bands, D″ and D*. The D* band is reported to originate from sp^3 orbitals, whereas the D″ band is related to the amorphous phase [22,23]. Based on the positions of the curves, the D* (D″) band for samples "A" and "B" are at 1190 (1535) and 1160 (1504) cm^{-1}, respectively. Moreover, at high wavenumbers, identical broad bands in the range between 2500–3200 cm^{-1} are observed in the two Raman spectra of the two sets of samples. This broad band is an overlap of the 2D (2720 cm^{-1}) and D + G (2920 cm^{-1}) bands. It is a known fact that in two dimensional carbon nanomaterials, the presence of such a broad band refers to the presence of edges, defects and sp^2 regions [24]. Although the two Raman spectra show similarities, their subtle divergence demonstrates the difference in the structure and the defects of the two carbon nanospheres samples. The changes in the D, D* and D″ bands intensities, the G bands positions, and the I_D/I_G, I_{D^*}/I_G and $I_{D''}/I_G$ ratios corroborate the previous statement. The difference between the in-plane crystallite sizes (L_a) of samples "A" and "B" shown in Table 2, and calculated by applying the Tuinstra–Koenig formula (1), where C(514.5 nm) = 4.37 nm [25,26], indicates also that

Table 2
The observed D and G band positions in cm^{-1}, I_D/I_G ratios of samples "A" and "B", and the calculated crystallite sizes obtained by the use of Eq. (1). The excitation wavelength used for Raman spectroscopy is 514.5 nm.

	D-band	G-band	I_D/I_G	L_a (nm)
Sample "A"	1340	1596	0.94 ± 0.06	4.643 ± 0.356
Sample "B"	1345	1587	1.06 ± 0.07	4.132 ± 0.262

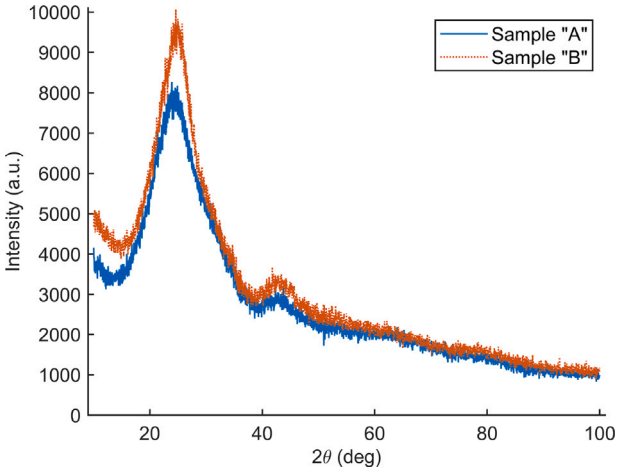

Fig. 4. XRD patterns of samples "A" and "B". The spectra reflect the diffraction planes (002) and (100).

Table 3
The calculated in-plane crystallite size (L_a) and inter-layer spacing (d_{002}) of samples "A" and "B" using the Scherrer equation and Bragg's Law.

	2θ (°)	β (rad)	L_a (nm)	d_{002} (nm)
Sample "A"	42.57	0.054	5.584	0.366
Sample "B"	42.82	0.067	4.541	0.357

the two samples possess different structures at the local scale.

$$L_a = C(\lambda) \times (I_D/I_G)^{-1} \quad (1)$$

The X-ray diffractograms of samples "A" and "B", shown in Fig. 4, are comparable to XRD patterns of carbon nanospheres reported in the literature [27–29]. The spectra are similar and characterised by two diffraction peaks, which correspond to the (002) and (100) planes of graphitic carbon materials [28,29]. The first peaks, (002), positioned at 24.24° and 24.88° for samples "A" and "B", respectively, are broad and of high intensities in comparison to the secondary peaks, (100), positioned at 42.57° and 42.82°, respectively. The predominant (002) and the weak (100) reflections indicate the presence of a graphite-like structures in the samples. In addition, the broadening and the absence of sharp peaks are a clear indication of structural disorder, hence the presence of amorphous carbon. From the previous statements, it is deduced that the crystallites of samples "A" and "B" are of intermediate structures between graphite and amorphous carbon [27]. The in-plane crystallite size (L_a) and the inter-layer spacing (d_{002}) of samples "A" and "B", deduced from the XRD patterns, are presented in Table 3. The crystallite sizes (L_a) are calculated by the use of the Scherrer Eq. (2), with λ, β and θ are the X-ray wavelength, the half-height width and the position of the (100) peak, respectively [30,31].

$$L_a = 1.84\lambda/\beta cos\theta \quad (2)$$

From Tables 2 and 3, the crystallite sizes (L_a) are observed to be similar. Therefore, it corroborates that samples "A" and "B" have different structures. In addition, the calculated inter-layer spacings (d_{002}) are in agreement with d_{002} values of carbon nanospheres reported in the literature [29].

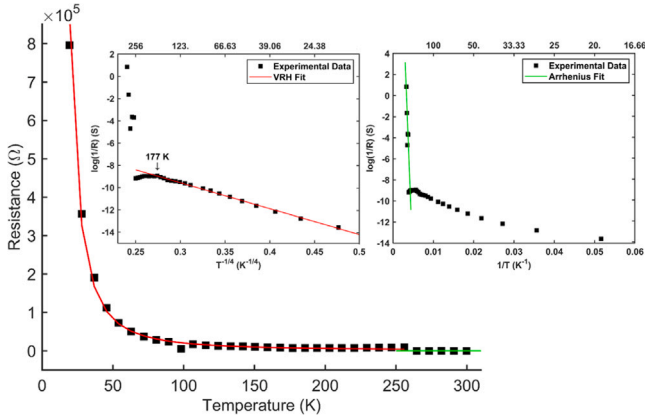

Fig. 5. The resistance, logarithm of the conductance as a function of the temperature in (K) and the fitted curves based on the 3D Variable Range Hopping (VRH) and Arrhenius equation. The absence of the data at low temperature (2–20 K) was related to the limitation of the PPMS, as very high resistance was measured within that temperature range. In the inset, the upper axis represents the temperatures in (K).

3.2. Resistance measurement/electrical properties

Resistance measurements were conducted over a temperature range between 2–300 K, and the logarithm of the inverse of the resistance (conductance) was plotted as a function of the inverse of the temperature. The relevant results of these measurements are presented in Fig. 5.

As seen in Fig. 5, the resistance of the carbon nanospheres network decreases non-linearly with the increase in temperature, which indicates a non-metallic and variable range hopping like behaviour of the sample. A logarithmic plot of the inverse of the resistance as a function of $T^{-1/4}$, shows that the electronic behaviour is described by three different sections. From 20 to 100 K, the resistance increases drastically with decreasing temperature, and the sample displays a semi-conducting behaviour, while between 250 and 300 K, the resistance shows a linear relationship with the temperature. In the interval between the above two ranges (100–250 K), the resistance shows a transition-like point and decreases steadily.

Similar semi-conducting features as that reported above were demonstrated in the literature for carbon microspheres [19,20] and carbon nanotubes networks [32]. Furthermore, it has been reported that these non-metallic characteristics arise from disorder and defects within the structure of the carbon nanomaterials and have been successfully explained by the Variable Range Hopping (VRH) model [19,20,32–34]. It must be noted that an important characteristic of the carbon nanospheres studied in the present work is that they are of the order of 200–400 nanometres in diameter in comparison to the micrometre size of carbon spheres in [19,20], and very importantly they have been produced without metal catalysts which could have affected previous conductivity results in the literature.

According to the VRH model, the conduction in disordered carbon materials is mediated by hopping of the charge carriers between localised electronic states near the Fermi level over an extended temperature range. The process of electron hopping from one localised state to another is thermally assisted by phonons which offer the necessary energy, which explains the temperature dependence with respect to lattice vibrations modes.

In the VRH model, the resistance is expressed as a function of the Mott temperature T_0, the localisation length L_c, and the density of states, $N(E_F)$, at the Fermi level [32,33,35].

$$R(T) = R_0\ exp(\frac{T_0}{T})^n \tag{3}$$

In this model, the Mott characteristic temperature T_0, and the exponent n (1/2 (1D), 1/3 (2D), 1/4 (3D)) represent the degree of disorder and the hopping dimension respectively, expressed as

$$T_0 = \frac{24}{\pi k_B L_c^3 N(E_F)} \tag{4}$$

From Fig. 5 ($R-T$ plot), the exponential escalation of the resistance with the decrease of the temperature reveals the strong localisation within the disordered carbon nanospheres network. In addition, at low temperature (2–180 K) the data are fitted with the 3D VRH model ($n = 1/4$), corresponding to the high disorder and the extreme localisation of the electronic states within the carbon nanospheres. Moreover, the estimated value of the Mott characteristic temperature, T_0, and the subsequently deduced density of states $N(E_F)$ were found to be 2.95×10^5 K and 3×10^{20} eV^{-1} cm^{-1}, respectively. These are in good agreement with those that have been reported in the literature for a localisation length of 10 Å [33]. L. Wang et al. [32] reported on distinct electrical properties of multi-walled carbon nanotubes and their conductivity results exhibit strong similarities with the data presented above. Three distinct regions were also observed, and the data were in good agreement with the VRH model.

At high temperatures, the experimental data of the conductance ($log(1/R)$) is observed to deviate considerably from the VRH fitting. It shows that the conduction cannot be explained by the VRH model, and a different mechanism of conduction is required. Therefore, the data for temperatures higher than 250 K were fitted using the Arrhenius Eq. (5) for thermal activation conduction, as seen in the inset of Fig. 5. The σ_0, E_a and k_B are the pre-exponential factor, the activation energy estimated to be 0.852 eV from the fit and the Boltzmann constant, respectively.

$$\sigma(T) = \sigma_0\ exp[-(\frac{E_a}{k_B T})] \tag{5}$$

3.3. Magnetic measurements/properties

The temperature dependence of the magnetic moments $\mu(T)$ was determined at field cooled conditions within a range of 2–300 K. The field cooled measurements were collected in both directions with the temperature decreased (cooling) and then increased (warming) at constant ramp rates. Moreover, the dependence of the magnetic moments (in emu) on applied magnetic field (H) in Oersted (Oe) was investigated. These measurements were performed at different temperatures from 2 K up to 310 K.

The temperature dependence of the magnetic moment $\mu(T)$ of samples "A" and "B" of the carbon nanospheres measured at 5 kOe in the temperature range $2 < T < 310$ K is shown in Fig. 6. Based on this graph, the FCC and FCW curves of both samples "A" and "B" are non-linear and the magnetic moment dependencies typically show monotonic exponential increase with decreasing temperature. The values of the magnetic moments $\mu(T)$ for sample "A" are positive with high magnitudes, while for sample "B" the magnetic moments are negative all along the x-axis indicating a diamagnetic behaviour.

It is interesting to note that a discrepancy between the FCC and FCW measurements, in the temperature range between 50 and 140 K for sample "A", was observed as seen in the upper-inset of Fig. 6.

In order to determine whether the observed positive value of the magnetic moment as a function of temperature for sample "A" correspond to ferromagnetic or ferrimagnetic behaviour, the magnetic moments $\mu(T)$ versus the magnetic field H were measured at temperatures 2, 10, 50, 100, and 300 K as shown in Fig. 7. All curves are characterised by a hysteresis at all temperatures with a clear saturation of the magnetic moments μ_{Sat} ($M_{Sat} = \mu_{Sat}$/mass) at high temperatures (>100 K). The magnetic moments reach saturation faster at high temperature, while at low temperature, the saturation of the magnetisation is greater at a larger magnetic field H.

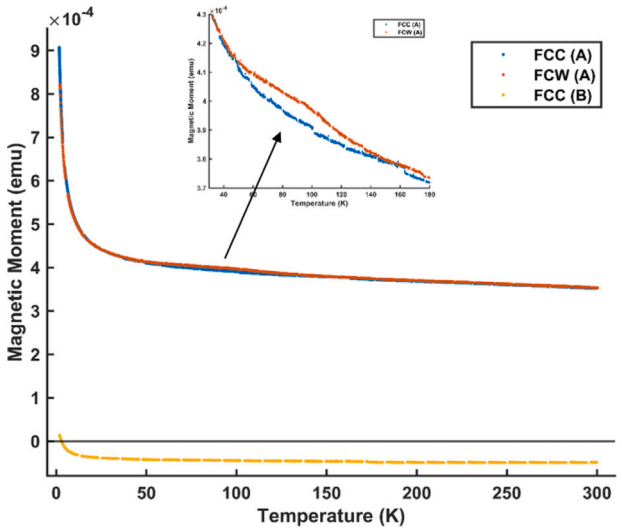

Fig. 6. The magnetic moment as a function of the temperature of the samples A and B at 0.5 T. (FCC) and (FCW) represent the field-cooled cooling and warming, respectively. The upper inset shows the FCC and FCW of sample "A" in a temperature range of 40–180 K.

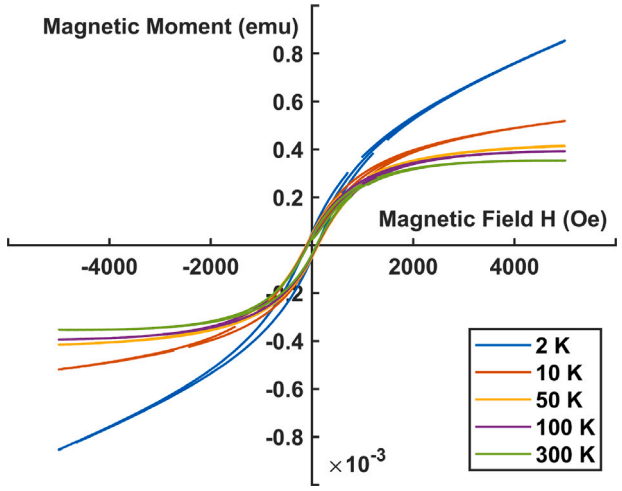

Fig. 7. The magnetic moments $\mu(H)$ in a range of −0.5–0.5 T of sample "A" at temperatures 2, 10, 50, 100, and 300 K. The curves show clearly the progress of the hysteresis at all temperatures.

Table 4
The coercivity, saturation and remanent magnetic moments generated from the hysteresis data at different temperatures.

Temperature (K)	$\mu_{Sat} \times 10^{-4}$ (emu)	H_c (Oe)	$\mu_r \times 10^{-5}$ (emu)
2	>8.5	−104	5.20
10	5.20	−111	4.80
50	4.16	−112.5	4.70
100	3.92	−92.5	3.95
300	3.54	−79	3.34

The remanent magnetisation M_r of the sample exhibits a similar trend as the magnetic saturation M_{Sat}. The remanent magnetisation M_r demonstrates a gradual increase as the sample temperature decreases. In contrast, the minimum magnetic coercivity H_c was recorded for a temperature of 50 K and the maximum was recorded at 300 K as shown in Table 4.

The magnetic moment measurements $\mu(H)$ on sample "B" (Fig. 8) at temperatures of 2, 10, 50, 100, 200, and 300 K confirm the conclusion drawn before from the $\mu(T)$ trend in Fig. 6. The curves exhibited a clear

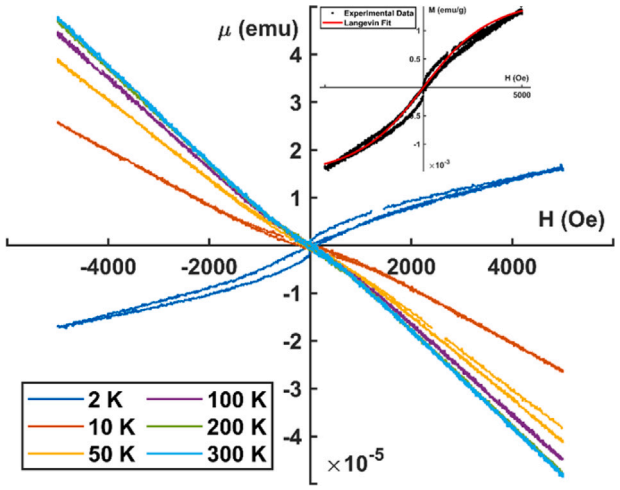

Fig. 8. The magnetic moments $\mu(H)$ of sample "B" at temperatures 2, 10. 50, 100, 200, and 300 K. The curves show the diamagnetism at temperatures between 10 to 300 K, and superparamagnetic behaviour at 2 K. The upper inset shows the fitted experimental data (Magnetisation in emu/g) at 2 K with the Langevin function.

diamagnetic behaviour above 2 K. In contrast, at 2 K the curve reveals a hysteresis with a very small width and a remanent magnetic moment of less than 3×10^{-5} emu.

Moreover, the mass susceptibility above 50 K was calculated from Fig. 8 to be $\sim -5.6 \times 10^{-7}$ emu g^{-1} Oe^{-1}. This value is in good agreement with the susceptibility range of $-(10^{-5}$–$10^{-7})$ emu g^{-1} Oe^{-1} for carbon allotropes exhibiting diamagnetic behaviour [13]. Also, the appearance of positive magnetic moments at very low temperatures (T < 10 K) could be attributed to the retention of isolated paramagnetic spins in the carbon mass [13], mostly from Fe impurities. In addition, the experimental data at 2 K can be fitted with the Langevin function (6) (upper inset in Fig. 8), which is used to explain the magnetism in superparamagnets and also is valid for classical spins [15].

$$M(H) = M_{Sat}[coth(x) - \frac{1}{x}] \quad (6)$$

where, $x = \mu B/(k_B T)$, where μ, B, k_B, and T are the magnetic moment, the magnetic field, the Boltzmann constant, and the temperature respectively, and M_{Sat} is the magnetisation saturation. From the fitted curve, the magnetic moment was derived to be equal to 21.5 μ_B.

In Figs. 7 and 8, the measurements point towards two distinctly different magnetic behaviours of the two different samples of carbon nanospheres investigated. With respect to $\mu(H)$, sample "A" is characterised by ferromagnetic behaviour with a clear hysteresis observed at all temperatures, while sample" B" exhibits diamagnetism except at 2 K at which a hysteresis with small width is observed. These results are unusual as bulk carbon materials are known to be diamagnetic, and also, the samples were synthesised with the same method under similar conditions.

The observed ferromagnetism in sample "A" might also be attributed to the presence of magnetic impurities, however, if these cannot account quantitatively for the entire effect, then the rest of the magnetisation must be related to magnetic moments induced within the carbon nanospheres.

In order to obtain a better understanding of the origin of ferromagnetism in the samples investigated, and to determine whether the contribution of the ferromagnetic behaviour is intrinsic or extrinsic, more evidence was needed other than the magnetisation measurements to supplement the reported results.

3.4. Trace magnetic impurities

The Inductively Coupled Plasma Mass Spectroscopy data, in Table 1, has shown that there exists only one magnetic impurity in the form of

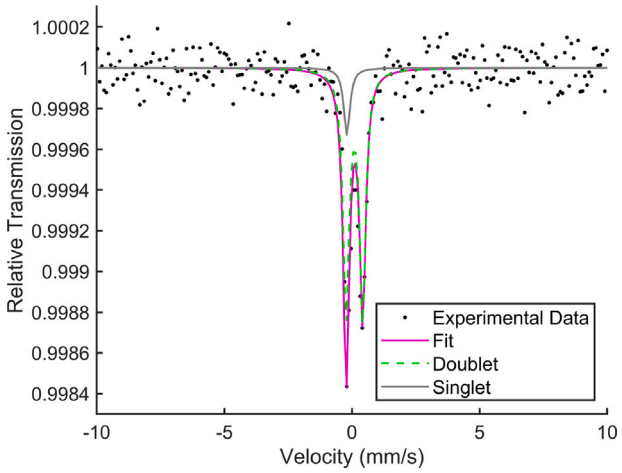

Fig. 9. The Mössbauer spectrum of sample "A" fitted with a Lorentzian singlet and quadrupole split doublet.

Fe in samples "A" and "B". The concentrations of Fe impurities were 126 ppm in sample "A" and 20 ppm in sample "B". Concentrations of other magnetic elements such as Ni and Co were very low and less than 3 ppm (Ni) or not detectable at the ppm level (Co) for the two samples. The Fe impurity within the carbon nanospheres forms most probably complexes of iron carbide or iron oxide.

The saturation magnetisation M_{Sat} for sample "A" was estimated by extrapolation from the measured magnetisation curves (Fig. 7), to be 7.4×10^{-2} emu g^{-1}. Given the amount of Fe impurity in the sample as measured by inductively coupled plasma mass spectroscopy (Table 1), the corresponding calculated magnetic saturation M_{Sat} values are expected to be of the order of 2.64×10^{-2} emu g^{-1} (1 ppm of Fe contributes with 2.2×10^{-4} emu g^{-1} [4]), by making the very general assumption that all Fe atoms of the impurity content are participating in the form of magnetic complexes. This value for sample "A" is still 2.8 times lower than the observed magnetisation and it indicates that Fe alone could not be the sole contributor to the magnetisation observed in these carbon nanospheres. Also, Fe impurity concentrations in the range between 20–100 ppm and uniformly distributed in a sample cannot contribute to the magnetisation, due to the large inter-atomic distances which results in the impossibility of exchange interaction [36].

3.5. Mössbauer spectroscopy

In order to investigate further the possible origins of the observed ferromagnetic signal, Mössbauer spectroscopy was performed on sample "A" using ^{57}Co as a radioactive source. As the concentration of Fe is extremely low, data were collected for more than five weeks (over 10000 counts) and the corresponding Mössbauer spectrum is presented in Fig. 9.

The spectrum is characterised by a weak signal in the form of a doublet around zero velocity with a large background. The signal is directly related to the presence of the iron element in the sample and confirms the reported results by inductively coupled plasma mass spectroscopy concerning the presence of Fe within the samples.

The Mössbauer spectrum was fitted with a combination of a Lorentzian singlet and quadrupole split doublet. The characteristic parameters of this fit are the isomer shift δ, quadrupole splitting ΔE_Q and linewidth Γ which are summarised in Table 5. The reported parameters of the fitted doublet are characteristic of Fe^{3+}. The quadrupole splitting is found to be large in comparison to ΔE_Q of $\alpha - Fe_2O_3$ bulk material (0.5 mm/s) [37]. It is suggested that the deduced ΔE_Q corresponds to particles of a diameter smaller than 10 nm [37]. In addition, the singlet corresponds to a non-ferromagnetic phase of Fe and the negative value of δ supports this statement [38] (see Table 5).

Table 5
The hyper-fine parameters deduced from the fits of the Mössbauer spectrum reported in Fig. 9, and the area fraction (A) of the spectral components.

Singlet			
δ (mm/s)		Γ (mm/s)	A (%)
−0.20 ± 0.03		0.29 ± 0.07	12
Doublet			
δ (mm/s)	ΔE_Q (mm/s)	Γ (mm/s)	A (%)
0.10 ± 0.01	0.65 ± 0.01	0.29 ± 0.01	88

By comparison to the Mössbauer analysis results obtained in the literature [37–39] with respect to Fe inclusions in carbon materials, the present spectrum and the inferred associated hyper-fine parameters from the fit strongly suggests that the observed signal is due to Fe^{3+} and is of non-ferromagnetic nature.

It is important to note that the Mössbauer spectrum is characterised by an absence of any magnetic split sextet signature which is a typical characteristic of ferromagnetic Fe structures as shown in the literature [37–39]. The Fe in the present samples therefore does not form ferromagnetic molecular complexes. This finding is important with respect to the clear ferromagnetic signal that has been observed for sample "A" using PPMS as it excludes the association of the observed ferromagnetism to Fe impurities. Also, it is important to mention that the Mössbauer spectrum was accumulated two times in order to check reproducibility and reliability and each time they produced identical results.

The appearance of the ferromagnetic behaviour depends on the existence of unpaired spins in the carbon nanostructures. It has been argued in the literature that such unpaired spins are introduced by dangling bonds, local change of hybridisation from sp^2 to sp^3, correlated electron behaviour and edge effects (zigzag edges) [36,40]. Moreover, unpaired electrons can be formed among the interconnections of the carbon nanostructures. Besides, topological disorder such as curvature in the surface and the formation of microstructures and defects (carbon vacancies and carbon adatoms) have been attributed as the origin of the ferromagnetic phases in carbon allotropes [14,15,36,41]. Experimental and theoretical studies have also suggested that hydrogen plays a major role in the inducement of magnetic ordering in carbon-based materials, through the formation of mono- and di-hydrogenated carbon atoms, as well as mono-hydrogenated edges [6–8,40,42,43]. Studies of the polymerisation of fullerenes reported that the observed ferromagnetism depends on the temperature and the duration of preparation of the samples [36]. Several reports on magnetism in carbon materials linked the magnetism to the presence of metallic impurities [44].

Regarding this work, the depicted ferromagnetism in the carbon nanospheres powder was verified to be intrinsic. The experimental data from inductively coupled plasma mass spectroscopy and Mössbauer spectroscopy of sample "A", supported by the calculation of the magnetisation indicates that the observed ferromagnetic behaviour originates from s-p symmetry unpaired electrons at structural defects rather than the d or f electrons of the magnetic impurities [1,7,14]. It is important to mention that ferromagnetism dominates, however it is not the sole contributor to the magnetic properties of sample "A" and a minor contribution from diamagnetism is expected.

The presence of such ferromagnetic behaviour can be associated with one or more of the explanations stated in the previous paragraph. It is highly likely that during the synthesis of the carbon nanospheres which consists of the pyrolytic decomposition of acetylene (C_2H_2) gas, mono- and di-hydrogenated carbon atoms may be formed in the process on the surface of the carbon nanospheres. The presence of hydrogen is stressed to be the origin of the magnetic ordering, as mentioned in several studies. Besides, the synthesised carbon nanospheress were undispersed forming in a necklace-like structure. Therefore, the ferromagnetism could be attributed to the existence of unpaired spins from the dangling bonds and zigzag edges within the interconnections of the

carbon nanospheres. In addition, the time of reaction and temperature of the synthesis may play a crucial role in the observed magnetic behaviour of the two samples.

4. Conclusions

In this study, the magnetic and electronic properties of carbon nanospheres grown with the chemical vapour deposition method were reported using a state-of-the-art physical property measurement system. Scanning electron microscope imaging, Raman spectroscopy and X-ray diffraction of the two investigated sets of carbon nanospheres, synthesised under slightly different conditions, revealed a difference in structure and size with a diameters distribution of approximately 200–400 nm and 400–500 nm. Inductively Coupled Plasma Mass Spectroscopy data showed the presence of ferromagnetic impurities such as Fe. The magnetic measurements of the two samples showed two different characteristics. In sample "A" clear ferromagnetism behaviour was observed, while in sample "B", diamagnetic behaviour was observed except at low temperature (<10 K), at which clear superparamagnetic behaviour is observed. The gathered evidence from inductively coupled plasma mass spectroscopy, Mössbauer spectroscopy, and the calculation of the saturation magnetisation showed that the observed ferromagnetism in the sample "A" is intrinsic and is not induced by the magnetic impurities introduced during the synthesis process.

Presently, it is difficult to elaborate on the origin of the observed ferromagnetic behaviour and it will become the main theme of future work with a series of new experiments and theoretical models. This intrinsic ferromagnetism in the carbon nanospheres is highly significant for medical applications such as magnetic drug delivery and hyperthermia treatment. These controlled drug carriers (carbon nanospheres) can target the tumour site guided by the magnetic field to release their loads. Another benefit of the intrinsic property of the carbon nanospheres is the non-involvement of the d and f elements in this process which represent a real danger to the human body.

Regarding the electrical properties, the network of carbon nanospheres exhibits a semiconducting behaviour, and was modelled and fitted with the 3D variable range hopping at a temperature range between 2–200 K. This finding is in agreement with work conducted on carbon nanotubes networks. It must be emphasised that in this case the samples were produced without metal catalysts and therefore the present measurements represent a clearer indication of the validity of the 3D variable range hopping model at low temperatures.

Declaration of competing interest

The authors declare that they have no known competing financial interests or personal relationships that could have appeared to influence the work reported in this paper.

Data availability

No data was used for the research described in the article.

Acknowledgement

DW would like to thank National Research Foundation, South Africa for funding through the NEP program (grant number UID: 116181).

References

[1] D. Li, Z. Han, B. Wu, D. Geng, Z. Zhang, Ferromagnetic and spin-glass behaviour of nanosized oriented pyrolytic graphite in Pb–C nanocomposites, J. Phys. D: Appl. Phys. 41 (11) (2008) 115005.

[2] Y. Murakami, H. Suematsu, Magnetism of C60 induced by photo-assisted oxidation, Pure Appl. Chem. 68 (7) (1996) 1463–1467.

[3] T.L. Makarova, B. Sundqvist, R. Höhne, P. Esquinazi, Y. Kopelevich, P. Scharff, V.A. Davydov, L.S. Kashevarova, A.V. Rakhmanina, Magnetic carbon, Nature 413 (6857) (2001) 716–718.

[4] P. Esquinazi, A. Setzer, R. Höhne, C. Semmelhack, Y. Kopelevich, D. Spemann, T. Butz, B. Kohlstrunk, M. Lösche, Ferromagnetism in oriented graphite samples, Phys. Rev. B 66 (2) (2002) 024429.

[5] P. Esquinazi, D. Spemann, R. Höhne, A. Setzer, K.-H. Han, T. Butz, Induced magnetic ordering by proton irradiation in graphite, Phys. Rev. Lett. 91 (22) (2003) 227201.

[6] K.-h. Han, D. Spemann, P. Esquinazi, R. Höhne, V. Riede, T. Butz, Ferromagnetic spots in graphite produced by proton irradiation, Adv. Mater. 15 (20) (2003) 1719–1722.

[7] P. Esquinazi, R. Höhne, K.-H. Han, A. Setzer, D. Spemann, T. Butz, Magnetic carbon: Explicit evidence of ferromagnetism induced by proton irradiation, Carbon 42 (7) (2004) 1213–1218.

[8] D. Spemann, K.-H. Han, P. Esquinazi, R. Höhne, T. Butz, Ferromagnetic microstructures in highly oriented pyrolytic graphite created by high energy proton irradiation, Nucl. Instrum. Methods Phys. Res. B 219 (2004) 886–890.

[9] H. Xia, W. Li, Y. Song, X. Yang, X. Liu, M. Zhao, Y. Xia, C. Song, T.-W. Wang, D. Zhu, et al., Tunable magnetism in carbon-ion-implanted highly oriented pyrolytic graphite, Adv. Mater. 20 (24) (2008) 4679–4683.

[10] T. Enoki, N. Kawatsu, Y. Shibayama, H. Sato, R. Kobori, S. Maruyama, K. Kaneko, Magnetism of nano-graphite and its assembly, Polyhedron 20 (11–14) (2001) 1311–1315.

[11] Y. Wang, Y. Huang, Y. Song, X. Zhang, Y. Ma, J. Liang, Y. Chen, Room-temperature ferromagnetism of graphene, Nano Lett. 9 (1) (2009) 220–224.

[12] Y. Wu, Y. Feng, Z. He, D. Yu, Y. Xue, X. Liu, L. Han, X. Zhao, X. Liu, Facile preparation of hydrogenated graphene by hydrothermal methods and the investigation of its ferromagnetism, Chin. Chem. Lett. (2021).

[13] R. Caudillo, X. Gao, R. Escudero, M. José-Yacaman, J.B. Goodenough, Ferromagnetic behavior of carbon nanospheres encapsulating silver nanoparticles, Phys. Rev. B 74 (2006) 214418.

[14] A.V. Rode, E.G. Gamaly, A.G. Christy, J.G. Fitz Gerald, S.T. Hyde, R.G. Elliman, B. Luther-Davies, A.I. Veinger, J. Androulakis, J. Giapintzakis, Unconventional magnetism in all-carbon nanofoam, Phys. Rev. B 70 (2004) 054407.

[15] D. Arčon, Z. Jagličč, A. Zorko, A.V. Rode, A.G. Christy, N.R. Madsen, E.G. Gamaly, B. Luther-Davies, Origin of magnetic moments in carbon nanofoam, Phys. Rev. B 74 (2006) 014438.

[16] Y. Kopelevich, R.R. da Silva, J.H.S. Torres, A. Penicaud, T. Kyotani, Local ferromagnetism in microporous carbon with the structural regularity of zeolite Y, Phys. Rev. B 68 (2003) 092408.

[17] A.G. Ciucă, C.I. Grecu, P. Rotărescu, I. Gheorghe, A. Bolocan, A.M. Grumezescu, A.M. Holban, E. Andronescu, Nanostructures for drug delivery: Pharmacokinetic and toxicological aspects, in: Nanostructures for Drug Delivery, Elsevier, 2017, pp. 941–957.

[18] A.A. Deshmukh, S.D. Mhlanga, N.J. Coville, Carbon spheres, Mater. Sci. Eng. R 70 (1–2) (2010) 1–28.

[19] K.C. Mondal, A.M. Strydom, Z. Tetana, S.D. Mhlanga, M.J. Witcomb, J. Havel, R.M. Erasmus, N.J. Coville, Boron-doped carbon microspheres, Mater. Chem. Phys. 114 (2–3) (2009) 973–977.

[20] W.P. Wright, V. Marsicano, J. Keartland, R. Erasmus, S. Dube, N. Coville, The electrical transport properties of nitrogen doped carbon microspheres, Mater. Chem. Phys. 147 (3) (2014) 908–914.

[21] W.-h. Lee, J.H. Moon, Monodispersed N-doped carbon nanospheres for supercapacitor application, ACS Appl. Mater. Interfaces 6 (16) (2014) 13968–13976.

[22] A.Y. Lee, K. Yang, N.D. Anh, C. Park, S.M. Lee, T.G. Lee, M.S. Jeong, Raman study of D* band in graphene oxide and its correlation with reduction, Appl. Surf. Sci. 536 (2021) 147990.

[23] S. Vollebregt, R. Ishihara, F. Tichelaar, Y. Hou, C. Beenakker, Influence of the growth temperature on the first and second-order Raman band ratios and widths of carbon nanotubes and fibers, Carbon 50 (10) (2012) 3542–3554.

[24] J. Prías-Barragán, K. Gross, H. Ariza-Calderón, P. Prieto, C. Di Giorgio, F. Bobba, A. Cucolo, Room-temperature ferromagnetism in oxidized-graphenic nanoplatelets induced by topographic defects, J. Magn. Magn. Mater. 524 (2021) 167664.

[25] F. Tuinstra, J.L. Koenig, Raman spectrum of graphite, J. Chem. Phys. 53 (3) (2003) 1126–1130, arXiv:https://pubs.aip.org/aip/jcp/article-pdf/53/3/1126/10966879/1126_1_online.pdf.

[26] A.C. Ferrari, J. Robertson, Interpretation of Raman spectra of disordered and amorphous carbon, Phys. Rev. B 61 (2000) 14095–14107.

[27] J. Kang, O.L. Li, N. Saito, Synthesis of structure-controlled carbon nano spheres by solution plasma process, Carbon 60 (2013) 292–298.

[28] D. Yuan, J. Chen, J. Zeng, S. Tan, Preparation of monodisperse carbon nanospheres for electrochemical capacitors, Electrochem. Commun. 10 (7) (2008) 1067–1070.

[29] A. Nieto-Márquez, A. Romero, J.L. Valverde, Carbon nanospheres: synthesis, physicochemical properties and applications, J. Mater. Chem. 21 (2011) 1664–1672.

[30] L.G. Cançado, K. Takai, T. Enoki, M. Endo, Y.A. Kim, H. Mizusaki, A. Jorio, L.N. Coelho, R. Magalhães-Paniago, M.A. Pimenta, General equation for the determination of the crystallite size La of nanographite by Raman spectroscopy, Appl. Phys. Lett. 88 (16) (2006) 163106, arXiv:https://pubs.aip.org/aip/apl/article-pdf/doi/10.1063/1.2196057/14659447/163106_1_online.pdf.

[31] B. Manoj, A. Kunjomana, Study of stacking structure of amorphous carbon by X-Ray diffraction technique, Int. J. Electrochem. Sci. 7 (4) (2012) 3127–3134.

[32] L. Wang, H. Wang, T. Datta, M. Yin, X. Tian, Distinct electrical effects of multi-walled carbon nanotubes in two composites, J. Appl. Phys. 116 (17) (2014) 173708.

[33] K.G. Raj, P.A. Joy, Cross over from 3D variable range hopping to the 2D weak localization conduction mechanism in disordered carbon with the extent of graphitization, Phys. Chem. Chem. Phys. 17 (24) (2015) 16178–16185.

[34] A. Imani, G. Farzi, A. Ltaief, Facile synthesis and characterization of polypyrrole-multiwalled carbon nanotubes by in situ oxidative polymerization, Int. Nano Lett. 3 (1) (2013) 1–8.

[35] M. Campos, B. Bello Jr., Mechanism of conduction in doped polyaniline, J. Phys. D: Appl. Phys. 30 (10) (1997) 1531.

[36] T. Makarova, Magnetic properties of carbon structures, Semiconductors 38 (6) (2004) 615–638.

[37] J. Niemantsverdriet, A. Van der Kraan, W. Delgass, M. Vannice, Small-particle effects in Mössbauer spectra of a carbon-supported iron catalyst, J. Phys. Chem. 89 (1) (1985) 67–72.

[38] P. Coquay, E. De Grave, R.E. Vandenberghe, C. Dauwe, E. Flahaut, C. Laurent, A. Peigney, A. Rousset, Mössbauer spectroscopy study of MgAl2O4-matrix nanocomposite powders containing carbon nanotubes and iron-based nanoparticles, Acta Mater. 48 (11) (2000) 3015–3023.

[39] A. Peigney, P. Coquay, E. Flahaut, R.E. Vandenberghe, E. De Grave, C. Laurent, A study of the formation of single-and double-walled carbon nanotubes by a CVD method, J. Phys. Chem. B 105 (40) (2001) 9699–9710.

[40] M. Maruyama, K. Kusakabe, S. Tsuneyuki, K. Akagi, Y. Yoshimoto, J. Yamauchi, Magnetic properties of nanographite with modified zigzag edges, J. Phys. Chem. Solids 65 (2–3) (2004) 119–122.

[41] A.W. Mombrú, H. Pardo, R. Faccio, O.F. de Lima, E.R. Leite, G. Zanelatto, A.J.C. Lanfredi, C.A. Cardoso, F.M. Araújo-Moreira, Multilevel ferromagnetic behavior of room-temperature bulk magnetic graphite, Phys. Rev. B 71 (2005) 100404(R).

[42] K. Kusakabe, M. Maruyama, Magnetic nanographite, Phys. Rev. B 67 (9) (2003) 092406.

[43] S. Gao, J. Dong, N. Luo, S. Grasso, J. Guo, L. Lei, J. Wen, S. Wang, A. Taallah, Y. He, et al., Ferromagnetic correlation in hydrogen doped highly oriented pyrolytic graphite, Diam. Relat. Mater. 109 (2020) 108030.

[44] J. Černák, G. Helgesen, A.T. Skjeltorp, J. Kováč, J. Voltr, E. Čižmár, Magnetic properties of carbon nanodisk and nanocone powders, Phys. Rev. B 87 (1) (2013) 014434.